Single Gold Bipyramid Nanoparticle Orientation Measured by Plasmon-Resonant Scattering Polarimetry

Cam Nhung Vu, Zakarya Ouzit, Clotilde Lethiec, Agnès Maitre, Laurent Coolen, Frédéric Lerouge, Julien Laverdant

Single Gold Bipyramid Nanoparticle Orientation measured by Plasmon-resonant Scattering Polarimetry

Nhung C.Vu[1,], Zakarya Ouzit[2], Clotilde Lethiec[2], Agnès Maître[2], Laurent Coolen[2], Frédéric Lerouge[3], Julien Laverdant[1,†]*

[1]Institut Lumière Matière, Université Claude Bernard Lyon 1, CNRS, Université de Lyon, F-69622 Villeurbanne, France

[2]Sorbonne Université, CNRS, Institut de NanoSciences de Paris, INSP, F-75005 Paris, France

[3]Univ Lyon, Ens de Lyon, CNRS, Université Lyon 1, Laboratoire de Chimie UMR 5182, F-69342, Lyon, France

Corresponding Authors

[†]E-mail: julien.laverdant@univ-lyon1.fr.

[*]E-mail: cam-nhung.vu@univ-lyon1.fr.

ABSTRACT. The 3D orientation of a single gold nanoparticle is probed experimentally by light scattering polarimetry. We choose high-quality gold BiPyramids (AuBPs) that support around 700 nm a well-defined narrow longitudinal Localized Surface Plasmonic Resonance (LSPR) which can be considered as a linear radiating dipole. A specific spectroscopic dark-field technique was used to control the collection angles of the scattered light. The in-plane as well as the out-of-plane angles are determined by analyzing the polarization of the scattered radiation. The data are compared with a previously developed model where the environment and the angular collection both play crucial roles. We show that most of the single AuBPs present an out-of-plane orientation consistent with their geometry. Finally, the fundamental role of the collection angles on the determination of the orientation is investigated for the first time. Several features are then deduced: we validate the choice of the analytical 1D model, an accurate 3D orientation is obtained and the critical contribution of the evanescent waves is highlighted.

TOC GRAPHICS

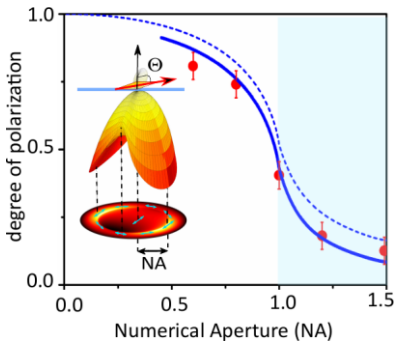

KEYWORDS. single gold bipyramids, plasmonics, scattering, polarization, orientation, evanescent waves.

Plasmonic NanoParticles (NPs) have been exploited in numerous applications due to their unique ability to concentrate light at the nanoscale[1]. For many applications, the knowledge of the nanoparticle orientation is required to maximize the desired properties. Among them, we can cite dipolar interactions and directional scattering. For instance, color routing has been achieved by manipulating the scattering diagram of two interacting metallic nanoparticles[2,3]. In assembled NPs, both optical and mechanical interactions strongly depend on the relative orientation between the NPs. The arising coupled modes have been widely studied and identified by optical measurements[4-6]. Another wide range of examples may be found in controlling the spontaneous emission of single emitters with NPs by tailoring their local electromagnetic environment with applications in nanoantennas[7,8], light – emitting devices[9], Raman spectroscopy[10], and biosensors[11-13]. It is then crucial that the emitter and the metallic NPs are well aligned in order to maximize their coupling.

In general, the orientation of a single nanoparticle is obtained experimentally from their radiation pattern or by polarization analysis. Various optical methods have been early applied to fluorescent molecules[14-16] and recently repeated for elongated metallic particles[12,17-22]. However, specific challenges still remain. For example, Fourier plane imaging[17,18] requires very sensitive detectors and a large number of photons to obtain sufficient signal-to-noise ratio. Defocused imaging[19,20] determines the orientation by just a slight displacement of an objective out of its focal plane. However, it is very sensitive to the alignment and aberrations of the experiment setup and cannot be applied to all cases (NPs deposited on a gold surface for example[28]). Another work reported a total internal reflection (TIR) scattering based on focused orientation and position imaging (FOPI) of gold nanorods[21]. This method has shown better signal – to – noise ratio but requires a gold substrate to enhance the out – of – plane component, thus limiting the applications of this technique. If we only focus on metallic NPs, polarimetric

analysis methods[12,20,22] have shown good precision without rigorous requirements as the radiation pattering imaging methods. One method is to split optical responses of metallic NPs into two orthogonal polarization directions to measure the optical anisotropy. However, the anisotropy measurement is only effective for the determination of the in – plane orientation. In this present study, we propose a scattering polarization analysis that could resolves 3D orientation of the NPs where the out – of – plane angle is effectively obtained from the scattering based Degree Of linear Polarization (DOP).

Gold BiPyramid nanoparticles (AuBPs) constitute an interesting model system for single-emitter light scattering. They exhibit a strong local field enhancement at their sharp end-tips, the so – called longitudinal Localized Surface Plasmon Resonance (LSPR), while the resonances along other directions (transverse modes) are usually negligible[23,24]. Furthermore, this longitudinal mode can be precisely tuned by changing the aspect ratio of the nanoparticles[25,26]. In spite of their excellent size and shape control and strong light-matter interactions, few reports, to our knowledge, have described the 3D orientation measurement of single AuBPs[17,20].

In this paper, for the first time, the 3D orientation of a single AuBP is precisely determined by polarization – based dark-field imaging. Here, we develop an original technic to precisely control the collection angle by Fourier – plane filtering of the scattering. The evolution of the scattering polarization with the objective numerical aperture allows us to validate a 1D dipole model that include the presence of the interface[28]. At the same time, the comparison between the experimental results and the theoretical calculations give access to the out-of-plane angle, with good precision and confidence (compared to other polarimetric measurements[28]). In particular, the critical role of the evanescent waves is clarified.

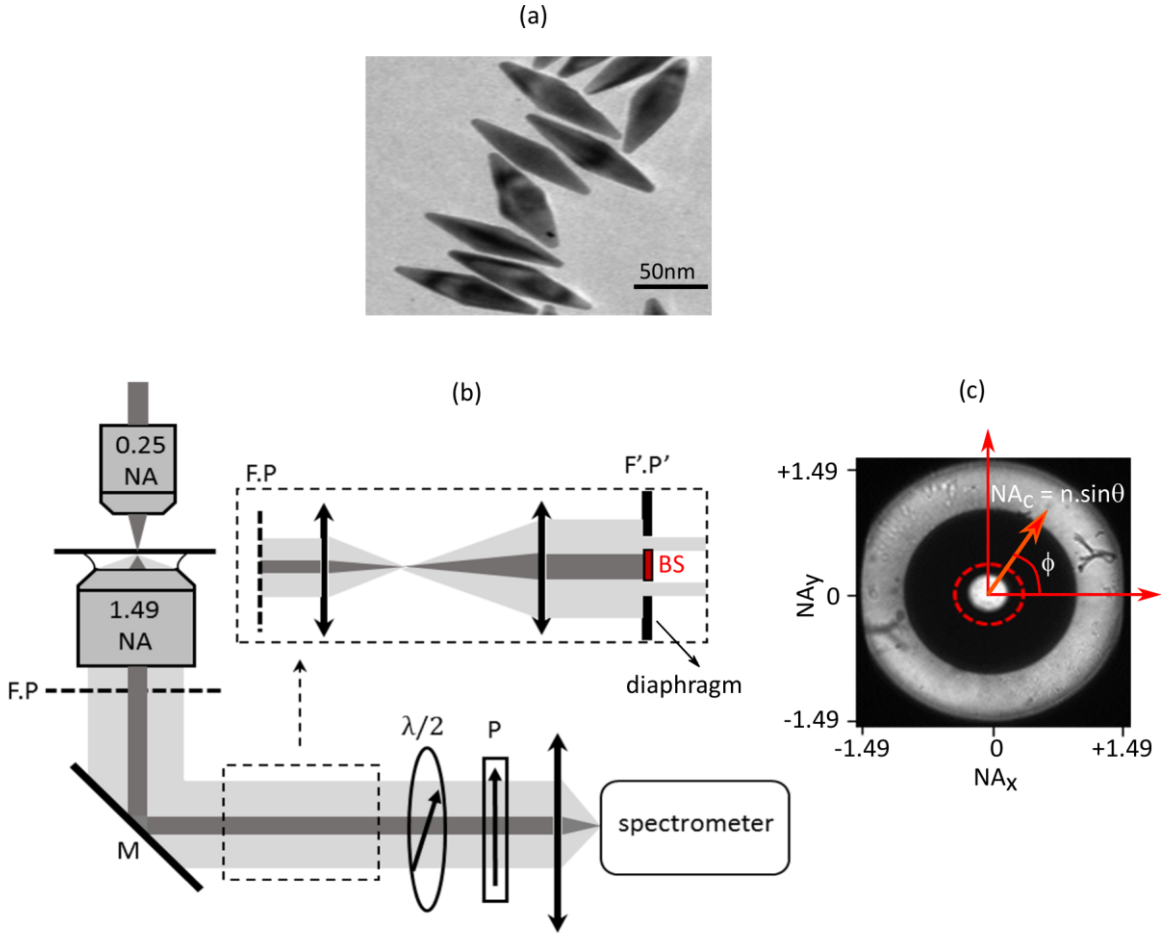

Figure 1. (a) TEM image of the AuBPs. (b) Schematic of the experimental setup: F.P denotes Fourier Plane. BS stems for Beam Stop. M, λ/2 and P are a silver mirror, half – wave plate, and polarizer plate, respectively. (c) CCD image of the F'.P' as a function of the numerical aperture of collection $NA_c = n.sin\theta$ and the tangential angle ϕ, where (θ, ϕ) are the spherical coordinates defining the solid angle of collection. The dashed circle corresponds to the size of the BS.

The synthesis procedure of the AuBPs was described in our previous article[24,25]. Their morphology has been studied by Transmission Electron Microscopy (TEM) (Figure 1a). The AuBPs have an average length of 100nm and width of 30nm with a very well – defined longitudinal resonance between 650 and 750nm measured in solution (Figure S2).

The sample is prepared by drop-casting the AuBPs solution on the glass substrate where its concentration has been adjusted to display well – separated nanoparticles (see SI Figure S1). Figure 1b depicts the experimental configuration to measure the orientation of an individual nanoparticle. The AuBPs are excited by the beam from a white lamp, focused by a 0.25 Numerical Aperture (NA) objective. Then, both the scattered light and the direct illumination are collected in transmission by an oil immersion objective (NA = 1.49). The matching refractive indices of the oil and the glass substrate ensure to acquire the scattering in a homogenous medium of index $n \sim 1.5$.

For dark – field imaging, a beam stop is placed in the Fourier plane of the collection objective. However, it is difficult to access the primary Fourier plane (F.P) of the objective, so a confocal system is employed to make an image of F.P at position F'.P' (dashed box, in Figure 1b). In order to explain this configuration, Figure 1c shows an image measured in the Fourier plane without the AuBPs. Each point in the Fourier plane can be associated to a direction of light radiation. The spherical angular coordinates (θ, ϕ) of this radiation direction can be obtained from the polar coordinates in the Fourier plane $(\phi, n.\sin\theta)$. We will refer to the radial coordinate $n.\sin\theta$ as the "collection numerical aperture" (NA_c). The radius of the disk corresponds to the maximum NA_c which is the oil objective numerical aperture (it is obtained by Fourier-imaging the light reflected by a bare glass substrate). The brighter beam in the center (around NA_c = 0.25) comes from the direct transmission of the incident white-lamp beam. When we study a gold nanoparticle, the radiation detected at collection $NA_c > 1$ is above the critical reflection angle $\sin^{-1}(1/n)$ and is excited by the evanescent components of the NP scattered field. The size of the beam stop is optimized at NA = 0.45 to cut off the direct transmission and keep only the scattered light. The signal is then captured by a CCD camera coupled with an Andor spectrometer (Kimera193i model).

The polarization analysis of the scattered light is then performed by combining a rotating half-wave plate λ/2 and a fixed polarizer plate (P). We chose this configuration so that the polarization does not change when entering the spectrometer. A calibration test has been conducted and showed that the depolarization of the overall experimental system is less than 3%. In the following step, we will present how the orientation of a single AuBP can be measured based on this experimental configuration.

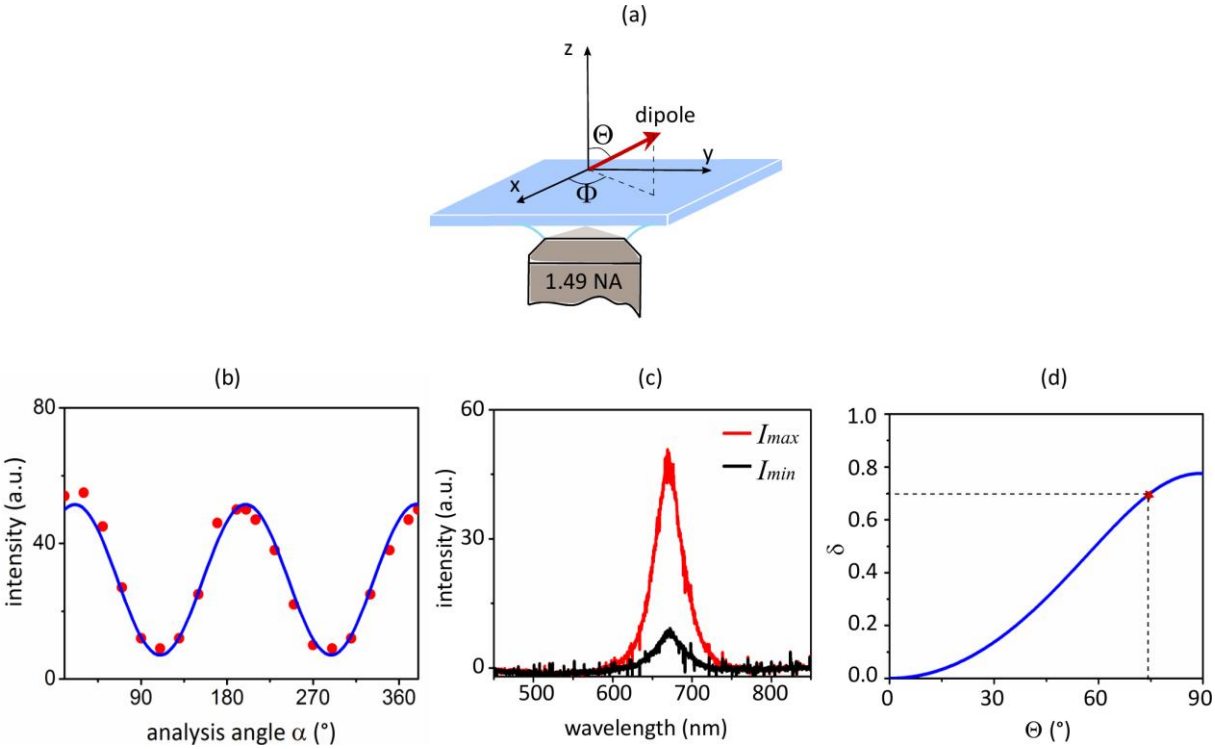

Figure 2: Polarimetric measurement of an isolated AuBP. (a) Coordinates system: (Θ, Φ) are the out – of –plane and in – plane orientations of the dipole. (b) The intensity of the scattering spectrum as a function of the polarization analysis angle α. The red dots are the experimental measurements. The blue line corresponds to the fit with eq 1. (c) Scattering spectrum for two orthogonal polarizations corresponding to maximum (I_{max}) and minimum (I_{min}) intensities. (d) Theoretical dependence of the Degree Of Polarization (DOP) δ on the dipole orientation Θ. The dashed line represents the experimental δ extracted from (c).

Theoretically, the calculation in the reference[27] has shown that:

- the in – plane dipole orientation Φ can be extracted from the partial Malus dependence of the polarized intensity I on the analysis angle α,

$$I(\alpha) = I_{min} + (I_{max} - I_{min})\cos^2(\Phi - \alpha), \quad (1)$$

- and the out – of – plane orientation Θ can be deduced from the measured degree of polarization (DOP) δ,

$$\delta = \frac{I_{max} - I_{min}}{I_{max} + I_{min}}, \quad (2)$$

provided that the dependence between δ and Θ is known theoretically.

We plot on Figure 2b the experimental dependence of the scattering intensity on the analysis angle α. The selected intensity oscillates between I_{max} and I_{min} (red dots) with a square-cosine dependence in good agreement with eq 1. This fit (blue line) gives the in – plane component Φ = 30° and the DOP δ = 0.72.

Alternatively the values I_{max} and I_{min} can be obtained directly by looking for the maximum and minimum of the scattering spectrum. Such spectra of a single AuBP are shown in Figure 2c. For this AuBP, we have a resonance at 670nm with a narrow FWHM of 40nm. This resonance is attributed to the longitudinal LSRP mode. Using eq 2, we calculate that δ = 0.7 for this particle, which is different by only 3% from the DOP extracted from Figure 2b. Therefore, for our following measurements, the DOP will be simply determined by taking the maximum and minimum intensities on the scattering spectrum.

Once δ is known, the orientation Θ is determined from the theoretical dependence δ(Θ)[28] as presented in Figure 2d. The model took into account the experimental parameters which have been described in the previous part. The emitter is located in air near a glass interface ($n = 1.5$) described as a semi-infinite medium. Given its 100-nm length, the radiating AuBP is modeled as a point dipole located at a distance z = $(100/2).cos\Theta$ (nm) from the glass surface.

The model calculates the emission polarization along each propagation direction, takes into account the transmission and redirection at the air-glass interface and sums the emission directions over the total objective numerical aperture. For the AuBP nanoparticle presented on Figure 2, based on this theoretical δ(Θ) curve and on the experimental value of δ, we find that Θ = 75°.

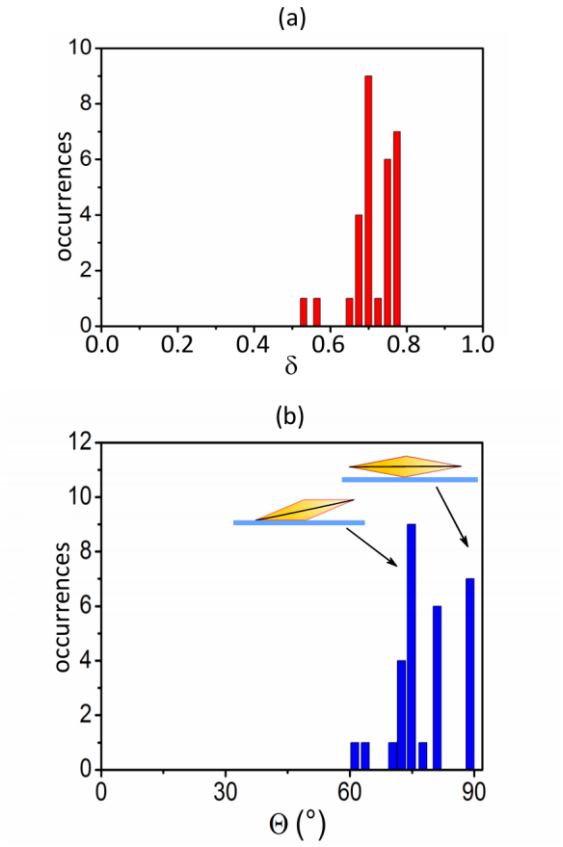

Figure 3: Histograms of (a) experimental values of δ, and (b) deduced orientations Θ, for 30 AuBP nanoparticles. Inset: Illustration of the AuBP orientations on the glass substrate.

With this procedure, we have measured δ for a selection of 30 AuBPs. Figure 3a presents the results as a distribution of δ between 0.5 – 0.8. By using the theoretical curve of δ(Θ) reported in Figure 2d, we deduce the orientation ranging from $\Theta \in [60°; 90°]$ in Figure 3b. The angle distribution is dominant around 70 – 80° which is consistent with a geometrical calculation of the AuBPs (Figure S5). The shape and the size distribution of the bipyramids as well as the

surface roughness have been measured to strengthen the hypothesis of our calculation (Figure S3 and S4). Besides, some orientations were found up to 90° and no orientation below 60° is observed. It indicates that the AuBPs do not have a tendency to deposit vertically on the substrate. This result is also consistent with other orientation studies where the AuBPs were found either tilted[17,29] by 15 – 20° from the substrate plane or horizontal[30] on the substrate.

From this statistic, the maximum δ recorded is 0.8. It is in good agreement with the theoretical calculation (Figure 2d). However, it seems to conflict with the polarization analysis of the AuBPs from other articles[24,25] where δ always reaches unity. The reason for this apparent inconsistency is that those other measurements were performed at lower numerical apertures, so that a much larger proportion of the scattered light was parallel to the dipole in-plane component. Therefore, in the following section, we will particularly evaluate the role of the numerical aperture in the polarization measurements.

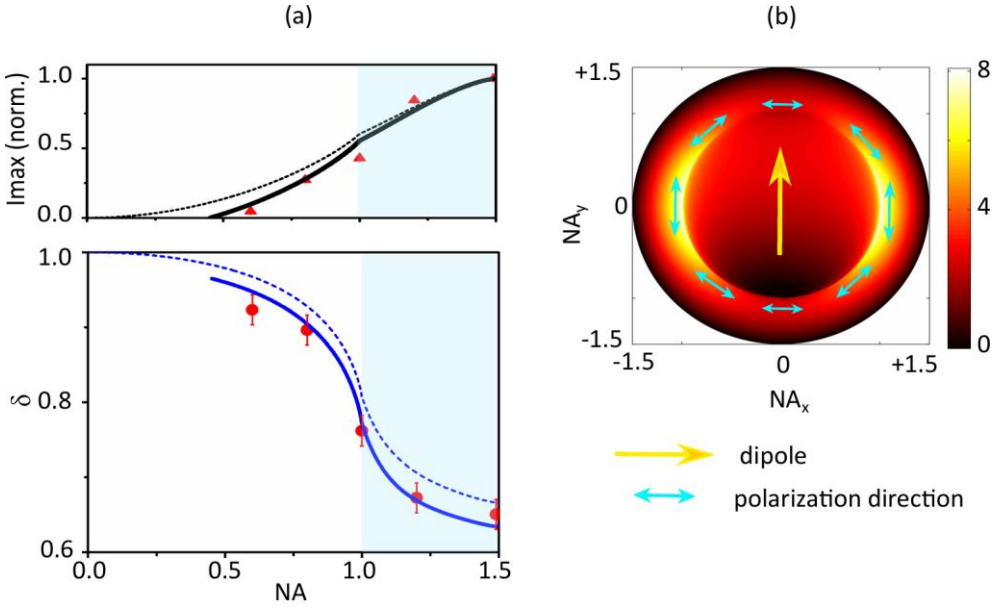

Figure 4: Evolution of the polarization measurement as a function of the objective numerical aperture: (a) degree of polarization δ (below) and normalized maximum intensity I_{max} (above). Red dots are experimental measurements on the same single AuBP. The lines show two cases

of theoretical calculations: NA ∈ [0.45; 1.49] with a 0.45-NA beam stop (solid lines) and NA ∈ [0; 1.49] without any beam stop (dashed lines). The blue zone corresponds to the $NA_c > 1$ values which collect part of the evanescent wave contribution. (b) Simulated scattering diagram in the Fourier plane.

To evaluate the dependence of the detected polarization on the objective numerical aperture (NA), we set a diaphragm at the F'.P' position as shown in Figure 1 in order to artificially reduce the NA. We, therefore, study δ as a function of NA for NA ∈ [0.45; 1.49]. Figure 4a presents the determination of δ for 5 values of the NA on the same AuBP. For each diaphragm radius (corresponding to a different NA), we measured δ as previously explained (see Figure 2). At the same time, we also measured the evolution of the scattering maximum intensity I_{max} with NA. The experimental results agree well with a theoretical fit (solid lines) and give an orientation $\Theta_{fit} = 69°$ with $\pm 2°$ of precision. These calculations have taken into account the presence of the beam stop at NA = 0.45. If we omit the presence of the beam stop and integrate over all collected angles down to θ = 0, only a slight difference is observed (dash line in Figure 4a below) because most of the scattering occurs at $NA_c > 1$. This shows that the polarization analysis protocol is not fundamentally modified by working in the dark-field mode.

Generally, the polarimetric measurements only obtain the out-of-plane angle Θ from one value of DOP. In a first step, we have deduced Θ with one DOP measurement (Figure 2 at NA=1.49) where the error of 3% in the experimental DOP lead to an error of 3° on Θ. However, it is difficult to choose an accurate model (1D or 2D degenerate dipole[27]) for fitting from only one DOP. The evolution of the DOP with NA (Figure 4) confirms that the choice of a 1D dipole model is in accordance with our data. With this final result, we found Θ with better confidence with an error of 2°-7°.

At the same time when opening the diaphragm, we observe an opposite tendency of the collected scattering and its degree of polarization. While the collection intensity increases, δ drops by 30%, especially near the critical region where $NA_c = 1$. This trend was also observed in the similar measurements of other AuBPs with different orientations (data not shown for clarity). In the meantime, even for horizontal AuBPs (Θ = 90°) where their polarization is supposed to be in the direction along the dipole axis, δ is not 1 but 0.8. To fully understand these behaviors, we need to correlate the polarization measurements to the scattering diagram.

For that purpose, we have calculated the radiation pattern of the dipole in Figure 4b in the Fourier plane. The center of the Fourier plane corresponds to a narrow solid angle of collection where the direction of the polarization is only linked to the projection of the dipole in the plane of the substrate resulting in δ = 1. When NA_c increases, the radiated field is no longer parallel to the dipole, and different directions ϕ show different field polarizations, so that the DOP, averaged over all collected angles, is lowered. This effect is stronger at important NA because the scattered field is radiated mostly at high angles, as the evanescent waves of the dipole near-field in air couple to the light propagative modes in glass[31] (blue zone, Figure 4a).

For now, we have proven that the DOP of a dipole is strongly influenced by the NA of observation. It raises a fundamental question: which NA is optimal for the orientation measurement of a dipole? According to the previous analysis (Figure 4), a large collection solid angle (NA > 1) is favorable because it obtains more information about the orientation. On the contrary, for a very narrow NA, only the in – plane angle Φ can be extracted as the DOP δ is always unity, regardless of the out-of-plane angle Θ (excluding the case of Θ = 0 which gives δ = 0 but which cannot be detected ($I_{max} = 0$) because there can be no radiation with wave vector parallel to the dipole).

However, in Figure 2d, we note that for NA = 1.49 objective, the DOP is constant around 0 for nearly-vertical dipoles Θ = [0 - 10°]. The same calculation of δ(Θ) has been done for other

numerical apertures (Figure S6). We found that a smaller NA allows a more accurate determination of Θ in cases where Θ is small, as the DOP varies more in the interval Θ = [0 - 10°]. However, because the detected total intensity is also smaller at low NA, the best NA of an objective to precisely determine a dipole orientation is a compromise between a strong δ(Θ) dependence and a good collection efficiency.

In conclusion, a dark-field scattering polarization analysis has been developed to measure the 3D orientation of AuBPs at the individual level. The out – of – plane component was precisely determined by taking advantage of the angular collection at the wide numerical aperture. We experimentally demonstrated that the more scattered light is collected, the more degree of polarization is decreased. In particular, the contribution of the evanescent wave is especially important in the orientation measurements. It is worth noting that the out – of – plane orientation can also be extracted from the evolution of the degree of polarization with the numerical aperture. Compared to other polarimetric methods, where the dipole orientation is determined from the degree of polarization only for one numerical aperture, our method combined with theoretical analysis strengthens our confidence on the determined orientation. The experimental technique we have proposed in this paper may be applied to more complex systems such as nanoparticle assembly where our method can discriminate polarization behaviors with the numerical aperture.

ASSOCIATED CONTENT

Supporting Information.

The distribution of the AuBPs on the substrates are displayed on dark-field images. Scattering spectrum of the AuBPs at a single level is compared to an ensemble measurement in the solution. We also present an orientation calculation based on the geometry of the AuBPs

correlated to the size distribution measured by TEM and the surface roughness deduced from profilometer analysis. Finally, theoretical calculations of the DOP are presented as function of the out – of – plane angle for different numerical apertures of collection (PDF).

AUTHOR INFORMATION

Corresponding Authors

[†]E-mail: julien.laverdant@univ-lyon1.fr.

[*]E-mail: cam-nhung.vu@univ-lyon1.fr.

Author Contributions

N.C.V and J.L designed, carried out the experiments and analyzed the data. F.L fabricated the gold bipyramids. Z.O, C.L, A.M and L.C developed the analytical model and performed the polarization simulations. N.C.V and J.L wrote the paper. All authors discussed the results and edited the paper.

Notes

The authors declare no competing financial interests.

ACKNOWLEDGMENT

The authors thank the USTH French consortium that supported this work. The financial support of Région Auvergne-Rhône Alpes (SCUSI Grant no 1700936601) is acknowledged.

REFERENCES

(1) Yu, H.; Peng, Y.; Yang, Y.; Li, Z. Y. Plasmonic – enhanced light – matter interactions and applications. *npj Computational Materials,* **2019**, *5,* 45.

(2) Shegai, T.; Chen, S.; Miljkovic, V. D.; Zengin, G; Johansson, P; Käll, M. A bimetallic nanoantenna for directional colour routing. *Nat. Commun*. **2011**, *2*, 481.

(3) Shegai, T.; Johansson, P.; Langhammer, C.; Käll, M. Directional Scattering and Hydrogen Sensing by Bimetallic Pd – Au Nanoantennas. *Nano Lett.* **2012**, *12*, 2464–2469.

(4) Tabor, C.; Haute, D. V.; El-Sayed, M. A. Effect of Orientation on Plasmonic Coupling between Gold Nanorods. *ACS Nano* **2009**, *3*, 3670–3678.

(5) Shao, L.; Woo, K. C.; Chen, H.; Jin, Z.; Wang, J.; Lin, H. Q. Angle – and Energy – Resolved Plasmon Coupling in Gold Nanorod Dimers. *ACS Nano* **2010**, *4*, 3053–3062.

(6) Li, X.; Lyu, J.; Goldmann, C.; Kociak, M.; Constantin, D.; Hamon, C. Plasmonic Oligomers with Tunable Conductive Nanojunctions. *J. Phys. Chem. Lett.* **2019**, *10*, 7093–7099.

(7) Esteban, R.; Teperik, T. V.; Greffect, J. J. Optical Patch Antennas for Single Photon Emission Using Surface Plasmon Resonances. *Phys. Rev. Lett.* **2010**, *104*, 026802.

(8) Akselrod, G. M.; Argyropoulos, C.; Hoang, T. B.; Ciraci, C.; Fang, C.; Huang, J.; Smith, D. R.; Mikkelsen, M. H. Probing the mechanisms of large Purcell enhancement in plasmonic nanoantennas. *Nature Photonis* **2018**, *8*, 835 – 840.

(9) Schientinger, S.; Barth, M.; Aichele, T.; Benson, O. Plasmon – Enhanced Single Photon Emission from a Nanoassembled Metal – Diamond Hybrid Structure at Room Temperature. *Nano Lett.* **2009**, *9*, 1694–1698.

(10) Shegai, T.; Brian, B.; Miljkovic, V. D.; Käll, M. Angular Distribution of Surface – Enhanced Raman Scattering from Individual Au Nanoparticle Aggregates. *ACS Nano* **2011**, *5*, 2036–2041.

(11) Rye, J. M.; Bonnet, C.; Lerouge, F.; Pellarin, M.; Lermé, J.; Parola, S.; Cottancin, E. Single gold bipyramids on a silanized substrate as robust plasmonic sensors for liquid environments. *Nanoscale* **2018**, *10*, 16094-16101.

(12) Chang, W. Q.; Ha, J. W.; Slaughter, L. S.; Link, S. Plasmonic nanorod absorbed as orientation sensors. *Proc.Natl.Acad.Sci. U.S.A.*, **2010**, *107*, 2781-2786.

(13) Lee, J.H.; Cheglakov, Z.; Yi, J.; Cronin, T. M.; Gibson, K. J.; Tian, B.; Weizmann, Y. Plasmonic Photothermal Gold Bipyramid Nanoreactors for Ultrafast Real-Time Bioassays. *J. Am. Chem. Soc.* **2017**, *139*, 8054–8057.

(14) Lieb, M. A.; Zavislan, J, M.; Novotny, L. Single-molecule orientations determined by direct emission pattern imaging. *J. Opt. Soc. Am. B*, **2004**, *21*, 1210-1215.

(15) Brokmann, X.; Coolen, L.; Hermier, J. P.; Dahan, M. Emission properties of single CdSe/ZnS quatum dots close to a dielectric interface. *Chemical Physics,* **2005**, *318*, 91–98.

(16) Ohmachi, M.; Komori, Y.; Iwane, A. H.; Fujii, F.; Jin, T.; Yanagida, T. Fluorescence microscopy for simultaneous observation of 3D orientation and movement and its application to quantum rod-tagged myosin V. *Proc. Natl. Acad. Sci. U.S.A.* **2012**, *109*, 5294-5298.

(17) Zhang, T.; Shen, H.; Lu, G.; Liu, J.; He, Y.; Wang, Y.; Gong, Q. Single Bipyramid Plasmonic Antenna Orientation Determined by Direct Photoluminescence Pattern Imaging. *Adv. Opt. Mater.* **2013**, *1*, 335-342.

(18) Huang, C.; Bouhelier, A.; Francs, G. C.; Bruyant, A.; Guenot, A.; Finot, E.; Weeber, J. C.; Dereux. A. Gain, detuning, and radiation patterns of nanoparticle optical antennas. *Phys. Rev. B.* **2008**, *78*, 155407.

(19) Xiao, L.; Quiao, Y. X.; He, Y.; Yeung, E. S. Three dimensional Orientational Imaging of Nanoparticles with Darkfield Microscopy. *Anal. Chem.* **2010**, *82*, 5268–5274.

(20) Lee, S. Y.; Han, Y.; Hong, J. W.; Ha, J. W. Single gold bipyramids with sharp tips as sensitive single particle orientation sensors in biological studies. *Nanoscale.* **2017**, *9*, 12060-12067.

(21) Ha, J. W.; Marchuk, K.; Fang, N. Focused Orientation and Position Imaging (FOPI) of Single Anisotropic Plasmonic Nanoparticles by Total Internal Reflection Scattering Microscopy. *Nano Lett.* **2012**, *12*, 4282–4288.

(22) Ha, J. W.; Sun, W.; Stender, A. S.; Fang, N. Dual-Wavelength Detection of Rotational Diffusion of Single Anisotropic Nanocarriers on Live Cell Membranes. *J. Phys. Chem. C* **2012**, *116*, 2766 – 2771.

(23) Anderson, L. J. E.; Mayer, K. M.; Fraleigh, R. D.; Yang, Y.; Lee, S.; Hafner, J. H. Quantitative Measurements of Individual Gold Nanoparticle Scattering Cross Sections. *J. Phys. Chem. C* **2010**, *114*, 11127–11132.

(24) Navarro, J. R. G.; Manchon, D.; Lerouge, F.; Blanchard, N. P.; Marotte, S.; Leverrier, Y.; Marvel, J.; Chaput, F.; Micouin, G.; Gabudean, A. M.; Mosset, A.; Cottancin, E.; Baldeck, P. L.; Kamada, K.; Parola, S. Synthesis of PEGylated gold nanostars and bipyramids for intracellular uptake. *Nanotechnology* **2012**, *23*, 465602.

(25) Navarro, J. R. G.; Manchon, D.; Lerouge, F.; Cottancin, E.; Lermé, J.; Bonnet, C.; Chaput, F.; Mosset, A.; Pellarin, M.; Parola, S. Synthesis, electron tomography and single-particle optical response of twisted gold nano-bipyramids. *Nanotechnology* **2012**, *23*, 145707.

(26) Lombardi, A.; Loumaigne, M.; Crut, A.; Maioli, P.; Fatti, N. D.; Vallée. F. Surface Plasmon Resonance Properties of Single Elongated Nano-objects: Gold Nanobipyramids and Nanorods. *Langmuir* **2012**, *28*, 9027–9033.

(27) Lethiec, C.; Pisanello, F.; Carbone, L.; Bramati, A.; Collen, L.; Maître. A. Polarimetry-based analysis of dipolar transitions of single colloidal CdSe/CdS dot-in-rods. *New J. Phys.* **2014**, *16*, 093014.

(28) Lethiec, C.; Laverdant, J.; Vallon, H.; Javaux, C.; Dubertret, B.; Frigerio, J. M.; Schwob, C.; Coolen, L.; Maitre, A. Measurement of Three-Dimensional Dipole Orientation of a Single Fluorescent Nanoemitter by Emission Polarization Analysis. *Phys. Rev. X.* **2014**, *4*, 021037.

(29) Burgin, J.; Liu, M.; Sionnest, P. G. Dielectric Sensing with Deposited Gold Bipyramids. *J. Phys. Chem. C* **2008**, *112*, 19279–19282.

(30) Pertreux, E.; Lombardi, A.; Florea, I.; Spuch-Calvar, M.; Gomez-Grana, S.; Ihiawakrim, D.; Hirlimann, C.; Ersen, O.; Majimel, J.; Treguer-Delapierre, M.; Hettich, M.; Maiolo, P.; Crut, A.; Vallée, F.; Fatti, N. D. Surface Plasmon Resonance of an Individual Nano-Object on an Absorbing Substrate: Quantitative Effects of Distance and 3D Orientation. *Adv. Opt. Mater.* **2016**, *4*, 567-577.

(31) Novotny, L.; Hecht, B. *Principle of Nano-Optics*; Cambridge University Press: Cambridge, U.K., 2006.